Direct numerical simulation of turbulent non-premixed combustion with realistic chemistry

By W. K. Bushe AND R. W. Bilger[1]

1. Motivation and objectives

Combustion is an important phenomenon in many engineering applications; combustion of hydrocarbons is still by far the most common source of energy in the world. In virtually every application of combustion processes, the flow in which the chemical reactions are taking place is turbulent. Furthermore, the combustion process itself is usually described by a very large system of elementary chemical reactions. These chemical kinetic mechanisms are usually extremely stiff and involve, for long-chain hydrocarbon species, perhaps hundreds of chemical species (which, if the combustion process is to be completely simulated, implies a need to solve hundreds of partial differential equations simultaneously). The governing equations describing the chemical composition are closely coupled to those describing the turbulent transport. Also, the chemical reaction rates are non-linear and strongly depend on the instantaneous composition and temperature. For these reasons, a full understanding of the many processes at work in devices such as furnaces, diesel engines, and gas turbines has been lacking.

In many devices of interest such as those mentioned above, the combustion takes place in what is known as the "non-premixed" regime. The fuel and oxidizer are initially unmixed, and in order for chemical reaction to take place, they must first mix together. In this regime, the rate at which fuel and oxidizer are consumed and at which heat and product species are produced is, therefore, to a large extent controlled by mixing. The nature of such flows lends itself to a particular variety of models which attempt to take advantage of this. These models describe mixing based on what is called the "mixture fraction", or the fraction of fluid which originated in the fuel stream; they attempt to either describe a steady state flame by a simple mapping operation—as in fast chemistry models (Bilger, 1980) and laminar flamelet models (Peters, 1984)—or incorporate reaction rates by expressing them as functions of the mixture fraction—as in the unsteady laminar flamelet model of Pitch and Peters (1998), the Conditional Moment Closure (CMC) model proposed independently by Klimenko (1990) and Bilger (1993a,b), and the Conditional Source-term Estimation (CSE) model of Bushe and Steiner (1998).

Work attempting to improve and validate models for turbulent combustion has been hampered by a lack of adequate experimental results. Experimental methods which might provide the necessary insight are also extremely expensive, difficult to perform, and still quite limited in the information they provide. Direct Numerical

1 The University of Sydney, Australia

Simulation (DNS) of the governing equations offers an alternative to experiments; however, such simulations are limited by available computer resources. Previous simulations have either been limited to extremely simple chemical kinetic mechanisms (Vervisch, 1992; Chen, *et al.*, 1992) or to two-dimensional flows (Smith, 1996; Chen & Echekki, 1996).

With the advent of new techniques for the systematic reduction of chemical kinetic mechanisms, new reduced kinetic mechanisms are now available which are still relatively simple but which retain sufficient complexity from the original mechanism to provide good predictions of flame structure and reaction rates. In a previous study which implements such a reduced mechanism in DNS (Swaminathan & Bilger, 1997 & 1998a), the flow was assumed to be incompressible so that effects of heat release on the flow were neglected. While the results of this study have been encouraging, validation of the CMC method against this constant property DNS data is not completely convincing. There is clearly a need to obtain DNS data using realistic chemical kinetics in turbulence where effects of the heat release on the flow are included.

In the present study, a reduced kinetic mechanism has been incorporated into a fully compressible DNS code. The results of the simulations will be used for the validation and, hopefully, improvement of current combustion models such as those mentioned above.

2. Accomplishments

2.1 Chemistry

The chemical kinetic mechanism that was used in the simulations is one representative of the oxidation of a methane/nitrogen mixture by an oxygen/nitrogen mixture. There are three reactions in the mechanism; the first two represent the oxidation of the methane (Williams, 1991), and the third represents the formation of nitric oxide and was obtained by putting the Oxygen free radical in the simple Zel'dovich into partial equilibrium. The reactions are:

$$Fuel + Oxi \rightarrow Int + Prod \tag{I}$$

$$Int + Oxi \rightarrow 2Prod \tag{II}$$

$$N_2 + Oxi \rightarrow 2NO \tag{III}$$

where *Fuel* is CH_4, *Oxi* is O_2, *Int* is $\left(\frac{4}{3}H_2 + \frac{2}{3}CO\right)$, and *Prod* is $\left(\frac{2}{3}H_2O + \frac{1}{3}CO_2\right)$.

In order to reduce computational costs and to make the mechanism more tractable for modeling purposes, the reaction rate expressions were simplified. The chemical kinetic mechanism was incorporated into a DNS code which solves the governing equations for fully compressible turbulent flow (Ruetsch *et al.*, 1995), based on the algorithms of Lele (1992) and Poinsot and Lele (1992). The implementation of the mechanism was thoroughly tested in one- and two-dimensional simulations; this work was described previously (Bushe *et al.*, 1997) and will not be discussed here.

2.2 Three-dimensional simulations

Having tested the implementation of the chemical kinetic mechanism and having established that simulation with turbulence was possible, a series of three-dimensional simulations were undertaken. Several limitations on initial and boundary conditions had been established in the two-dimensional tests.

For the simulation results to be useful for the purpose of model validation, it was clear that the bulk pressure in the domain would have to remain constant. In order to ensure this, fluid had to be allowed to leave the domain; therefore, it was necessary to use partially non-reflecting outflow boundary conditions (Poinsot & Lele, 1992) for at least one boundary. An additional constraint was then that the reaction rates at any such a boundary was required to be zero; otherwise, these boundary conditions become ill-posed. Also, because the chemical kinetic rates depend on the hydrogen free radical concentration, the mechanism cannot auto-ignite; therefore, the fields had to be initialized such that at least some chemical reaction is already underway.

The species mass fractions were initialized in the one-dimensional simulations by first defining the mixture fraction as a linear combination of mass fractions such that the chemical source term in its transport equation is zero:

$$Z = \frac{60Y_{Fuel} - 60Y_{Oxi} - 36Y_{Prod} - 32Y_{\mathrm{NO}} + 18}{27}. \tag{1}$$

The mixture fraction was initialized with the analytical solution to the diffusion equation for a semi-infinite slab of fuel mixing with a semi-infinite slab of oxidizer,

$$Z(x,t) = \mathrm{erf}\left(\frac{x}{\sqrt{4\mathcal{D}t}}\right), \tag{2}$$

at an arbitrary time, chosen such that the reaction zone would be sufficiently resolved with the available number of grid points. Mass fractions for each species were then calculated by assuming that an arbitrary fraction of moles for each of reaction I and II had reacted to completion. This assumption also allowed for the calculation of the heat released as a function of mixture fraction, from which the temperature field can be calculated. The initial velocity was zero, and both boundaries in the one-dimensional simulations allowed for partially reflecting out-flow.

The mass fraction, temperature, density, and velocity fields for the three-dimensional simulations were then initialized by using a stabilized one-dimensional flame solution. By placing a stable flame in the middle of the three-dimensional domain, the time until the reaction zone (the region of the flow in which chemical reaction takes place) reached a boundary could hopefully be maximized. The placement of the flame is depicted in Fig. 1.

Initial turbulent velocity fluctuations were obtained by using a pseudo-spectral code (Ruetsch & Maxey, 1991) to solve the governing equations for incompressible flow and forcing a periodic, three-dimensional flow field on a 120^3 grid from quiescence until its statistics became stationary. Two identical 120^3 boxes were placed

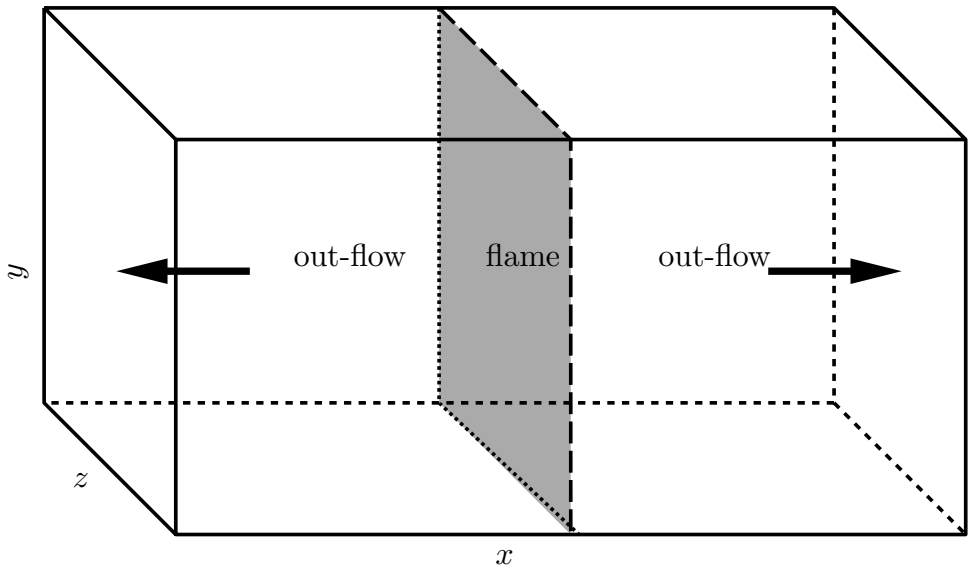

FIGURE 1. Depiction of initial flame placement.

next to each other to fill out the $120 \times 120 \times 240$ domain; periodic boundary conditions were retained for the y and z directions and out-flow boundaries used in the x direction as shown in Fig. 1. The turbulent fluctuations near the out-flow boundaries were filtered to zero to avoid potential generation of unphysical vorticity. The incompressible turbulent fluctuations were taken to be fluctuations in the momentum; thus, the turbulent velocity was divided by the density so as to satisfy

$$\frac{\partial(\rho u_i)}{\partial x_i} = 0,$$

in the initial field. The resulting turbulent velocity field was added to the velocity field induced by dilatation in the one-dimensional flame.

2.3 Results

Six sets of data have been produced. Two simulations were run for 90 time units, and the remainder were run only for 20 time units. These additional simulations were run to provide a larger ensemble of points from which to extract statistics. In each simulation the same initial flame was used, but the initial velocity field was either shifted or rotated such that the flame saw the same velocity field in a statistical sense but underwent a very different evolution. In all cases, data was stored for every 2.5 non-dimensional time units so that the evolution of the flow and scalar fields could be studied. The data stored included the density, the temperature, the mass fractions of Fuel, Oxidizer, Intermediate, Product and NO, and the velocity in each direction for every point in the domain.

2.3.1 Visualization of slices

In Figs. 2–4, eight different properties are visualized for a single plane oriented normal to the flame brush. These figures show the properties taken from one simulation at three different times (7.5, 15.0, and 30.0 time units). The properties

shown are summarized in Table 1, along with a legend to the colors in Figs. 2-4. The minima and maxima of the properties are kept the same for all three figures to allow direct comparison between them. Superimposed on these plots are isopleths of mixture fraction. The black lines are spaced at intervals of mixture fraction of 0.1, and the white line is the isopleth of the stoichiometric mixture fraction of 1/3. The gas at the right-hand edge of the figures is pure fuel (where the mixture fraction has a value of unity), and the gas at the left-hand edge of the figures is pure oxidizer (where the mixture fraction has a value of zero).

sub-figure	Property	Minimum (white)	Maximum (black)
a	χ	0	0.0125
b	T	300K	2000K
c	Y_{Int}	0	0.032
d	Y_{H}	0	0.0024
e	$\dot{\omega}_{\mathrm{I}}$	0	6.5×10^{-5}
f	$\dot{\omega}_{\mathrm{II}}$	0	6.0×10^{-5}
g	Y_{NO}	0	1.4×10^{-8}
h	$\dot{\omega}_{\mathrm{III}}$	0	2.3×10^{-5}

Table 1. Legend for Figs. 2, 3, and 4.

In Fig. 2, there is a peak in scalar dissipation evident, which coincides with a saddle point in the temperature. There is considerable fine-scale structure in the scalar dissipation. In the middle of the slice, there is a fairly large region in which the scalar dissipation along the stoichiometric isopleth is very low; it is in this region where the temperature is a maximum. This region also coincides with the maximum production rate of Nitric Oxide. Furthermore, the Intermediate and Nitric Oxide mass fractions also peak here. The Hydrogen radical, however, peaks in a region of moderately high scalar dissipation. Neither of reactions I or II show any sign of local extinction at this early time in the simulation; however, there are in both reaction rates double peaks, which may indicate turbulent structure within the reaction zone, although it is more likely a consequence of out-of-plane folding. Regardless, it would be difficult to describe the flame shown in this figure as being locally one-dimensional.

In Fig. 3, the peak in scalar dissipation which was apparent in Fig. 2 has become larger in magnitude and has been transported by the flow. The scalar dissipation still exhibits fine-scale structure. The saddle point in the temperature still coincides with the peak in scalar dissipation and has become deeper. The region of low scalar dissipation where the temperature is high has become larger, and the maximum temperature is slightly higher here. The Intermediate and Nitric Oxide mass fractions as well as the Nitric Oxide production rate all peak in this region. Interestingly, the Intermediate species mass fraction nearly vanishes at the location of the peak in scalar dissipation, as does the mass fraction of the Hydrogen radical,

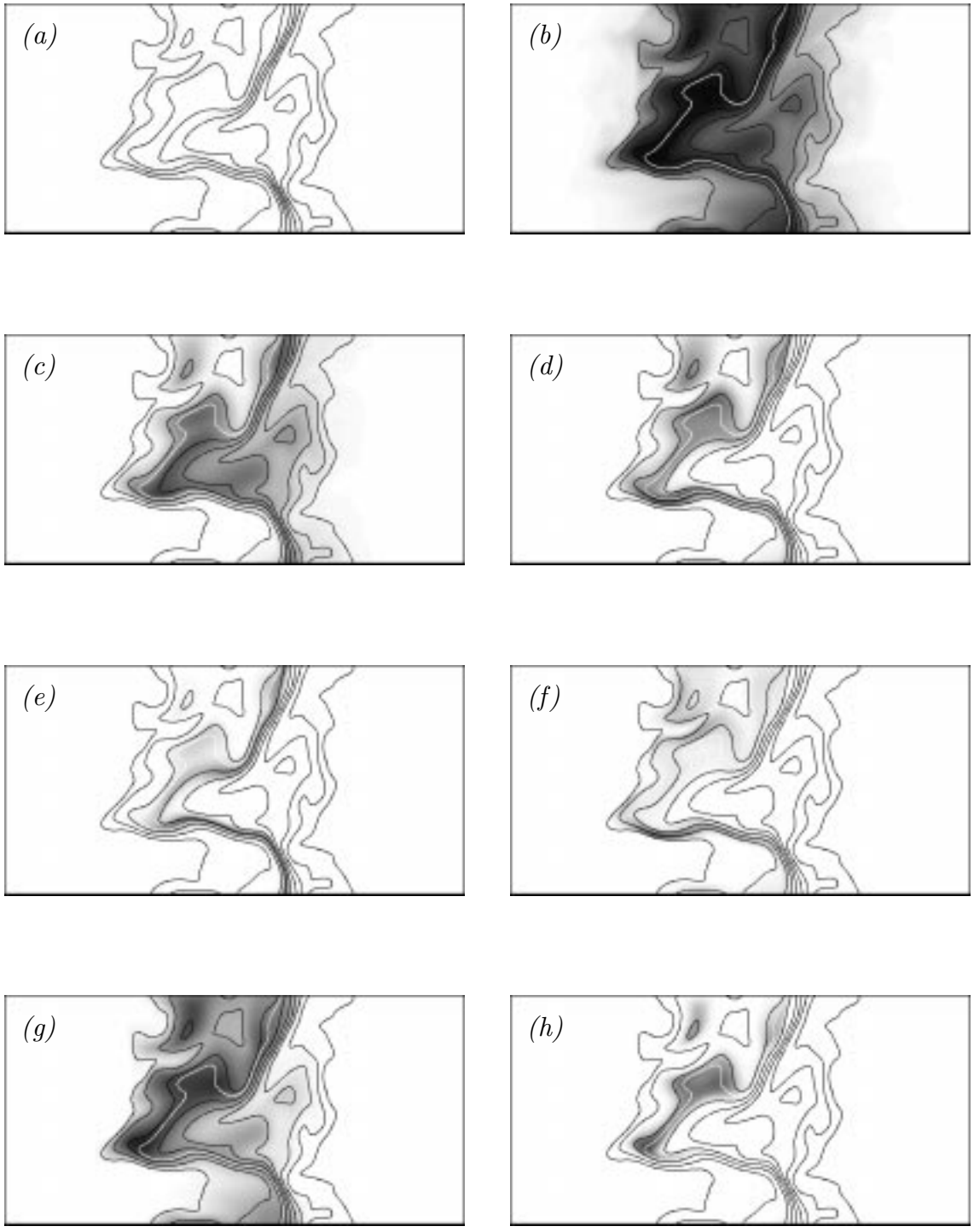

FIGURE 2. Visualization of properties on a slice through the three-dimensional domain after 7.5 acoustic time units: a) Scalar dissipation, b) Temperature, c) Mass fraction of Intermediate, d) Mass fraction of Hydrogen radical, d) Reaction rate I, e) Reaction rate II, f) Mass fraction of Nitric Oxide, g) Reaction rate III. See Table 1 for legend.

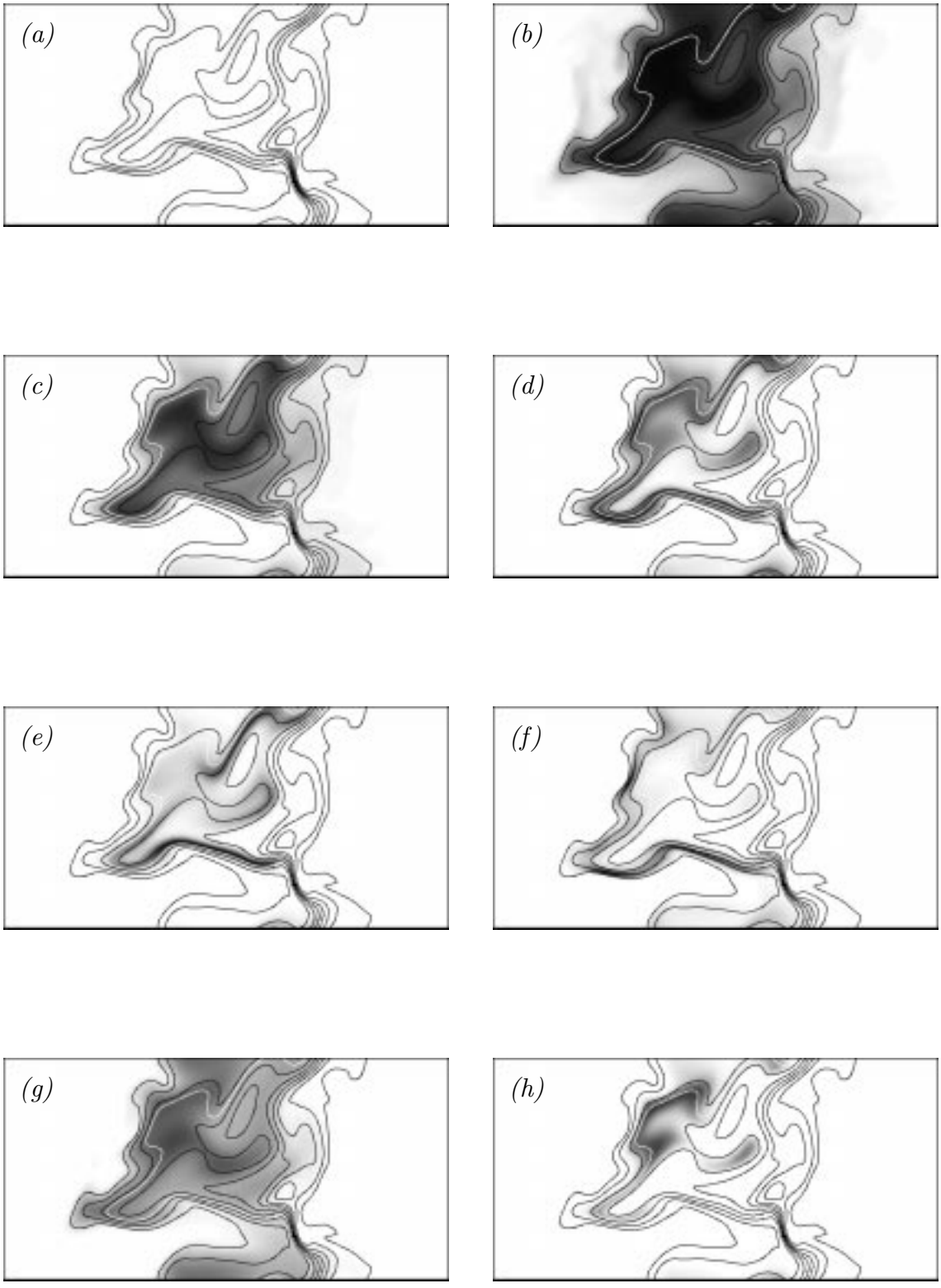

FIGURE 3. Visualization of same properties shown in Fig. 2 after 15.0 acoustic time units. See Table 1 for legend.

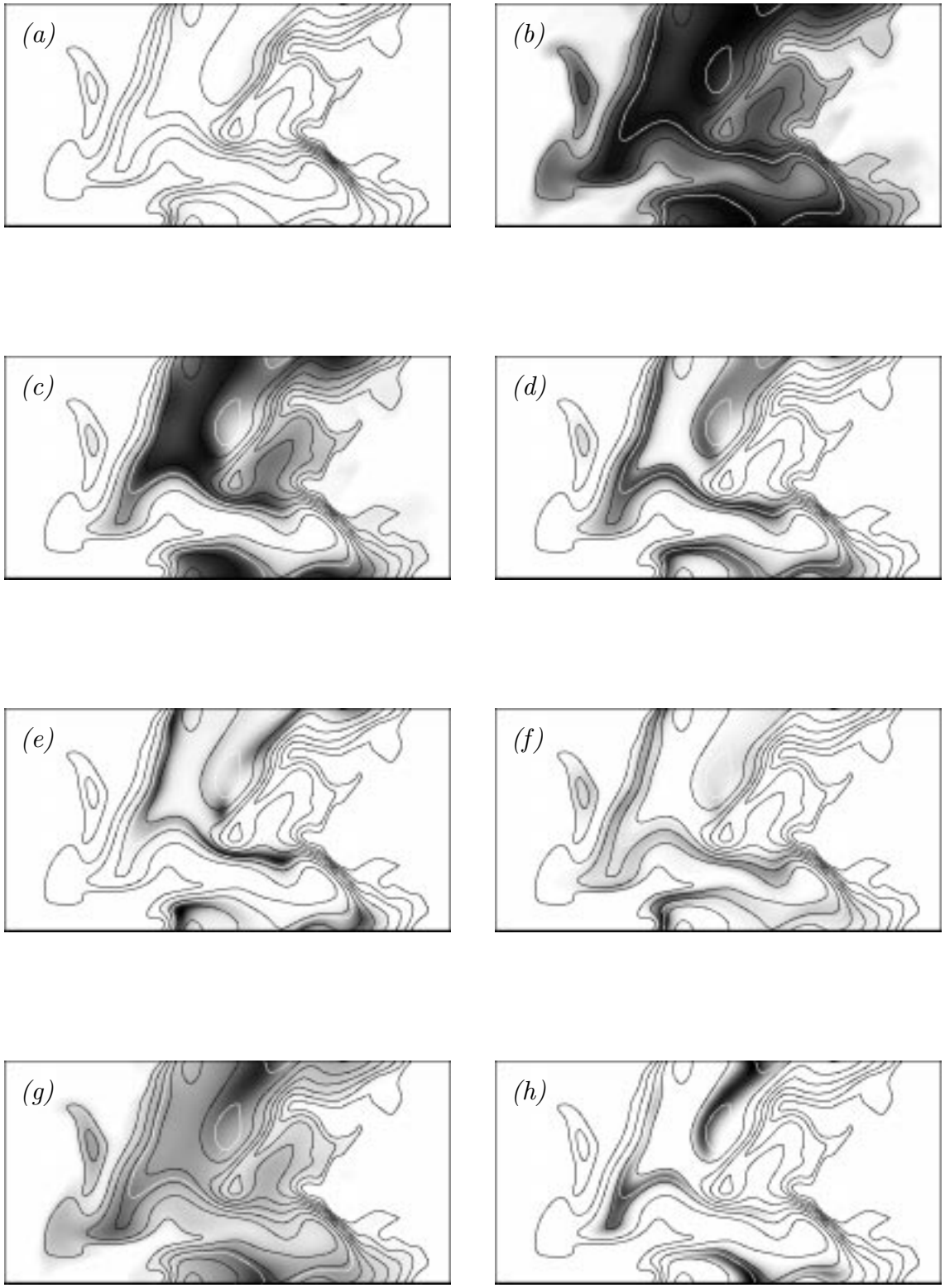

FIGURE 4. Visualization of same properties shown in Fig. 2 after 30.0 acoustic time units. See Table 1 for legend.

even along the stoichiometric isopleth of mixture fraction. This, coupled with the low temperature at this spot, has the effect of extinguishing the rates of reactions I and II; that is, the local reaction rates are more than an order of magnitude lower than they are at other locations with the same stoichiometry; this is what is known as local extinction. At this later time, reaction I is significant in a very broad region in space where the scalar dissipation is low (that the scalar dissipation is low here indicates that this is not merely a consequence of out-of-plane folding); furthermore, there is also a pocket of unreacting gas surrounded by reacting gas.

In Fig. 4, the peak in the scalar dissipation has been convected further to the right, but the peak is lower in magnitude. The structure in the scalar dissipation field is starting to exhibit somewhat larger scales than was seen at the earlier times. The temperature field still peaks in a region of very low scalar dissipation, and the saddle point in temperature associated with the peak in scalar dissipation has become even lower. The Intermediate mass fraction and the rate of reaction II are both very low in this region, and the Hydrogen radical mass fraction and rates of reactions I and III are all negligibly small. Peaks in the Nitric Oxide mass fraction are at the same locations as peaks in the rate of reaction III; these coincide with peaks in the temperature.

2.3.2 Scatter plots

Figure 5 gives scatter plots of the scalar dissipation, temperature, and mass fractions of Oxidizer, Fuel, Intermediate, and Hydrogen radical as functions of the mixture fraction for the simulation discussed above at a time of 15.0 time units. The scalar dissipation shows considerable scatter with a peak at a mixture fraction around 0.5. The peak scalar dissipation in the turbulent flow at this time is over 200 times the peak in the original laminar flow. In the plots of the temperature and the Fuel, Oxidizer, Intermediate, and Hydrogen radical mass fractions, the laminar flame with which the simulation was initialized is superimposed on the scatter plots. Most of the points in the temperature scatter plot lie below the initial flame, which is an effect of the increased scalar dissipation caused by turbulent mixing. Almost all of the points in the oxidizer and fuel mass fractions are higher above the curves of the initial flame, as are most of the points in the Hydrogen radical mass fraction plot. In this last plot, however, there are still a few points below the laminar flame curve; these are points that lie in regions of local extinction such as that discussed above. The Intermediate species mass fraction exhibits the most scatter of the mass fraction plots; however, the bulk of the points lie close to the laminar flame curve.

2.3.3 Turbulence statistics

While the field used to initialize the velocity in the turbulent simulations came from an isotropic simulation, the mixture fraction was initialized with an anisotropic field, and the turbulent velocity fluctuations were adjusted using the initial laminar flame density. Also, the viscosity was taken to be a function of the temperature, and the temperature had, as seen in the previous section, substantial variation even as a function of mixture fraction. Therefore, the initial velocity field was strongly anisotropic in the direction across the layer. As such it is difficult to describe the

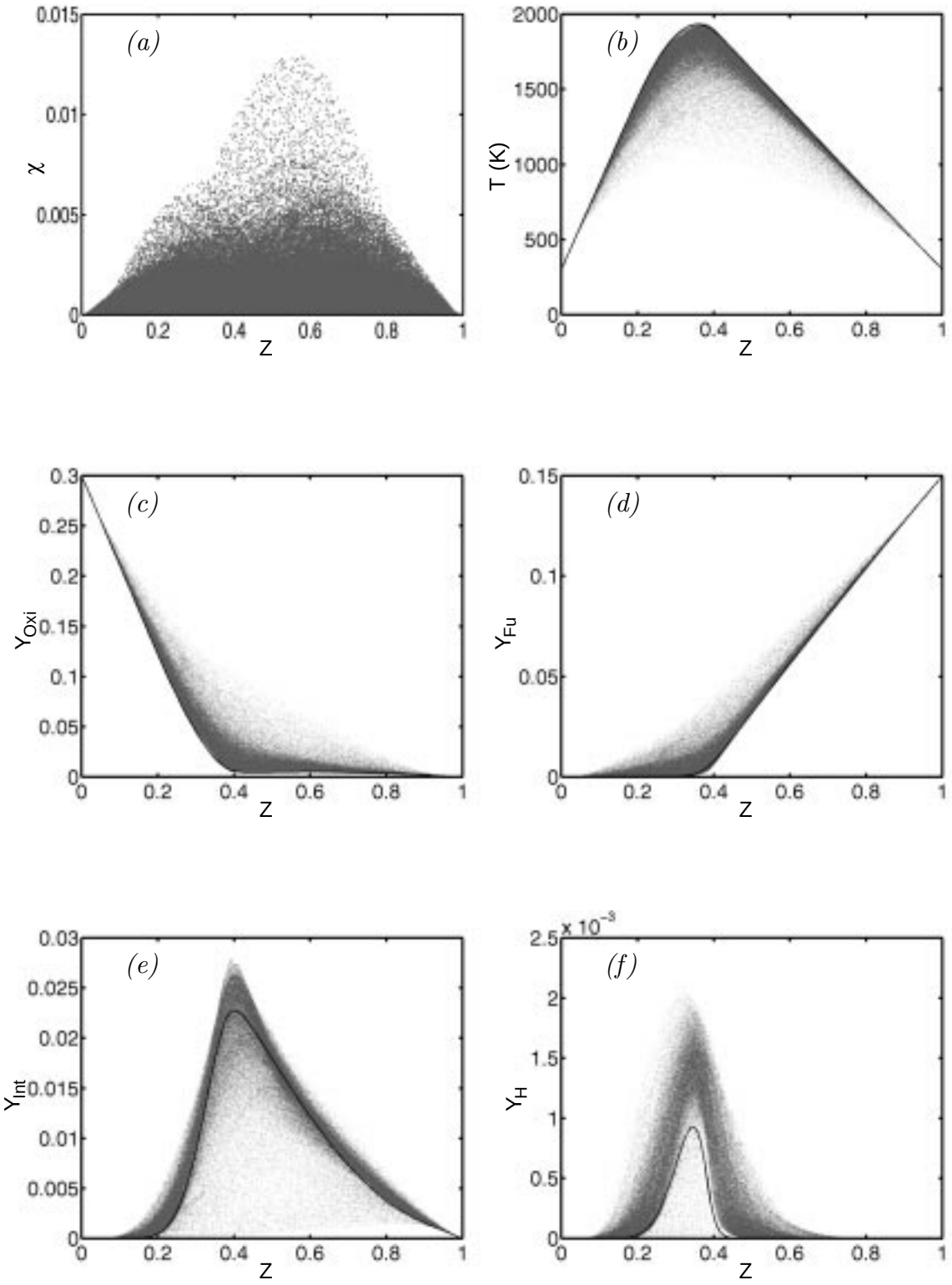

FIGURE 5. Scatter plots of a) Scalar dissipation, b) Temperature, c) Mass fraction of Oxidizer, d) Mass fraction of Fuel, e) Mass fraction of Intermediate and f) Mass fraction of hydrogen radical. Solid lines are initial laminar flame profiles.

characteristics of the flow using statistics. In order to examine the characteristics of the flow field, statistics were taken on planes normal to the direction of anisotropy in the mixture fraction field; that is, properties were averaged together on planes normal to the x direction. One unfortunate consequence of this is that there are only 120^2 points on each plane, which may mean that the statistics on these planes are not properly converged.

The Taylor microscale is defined by Tennekes and Lumley (1992) as

$$\lambda = \sqrt{\frac{10 \cdot \widetilde{\nu} \cdot \widetilde{k}}{\widetilde{\epsilon}}}$$

where $\nu = \frac{\overline{\rho\nu}}{\overline{\rho}}$ is the Favre averaged kinematic viscosity,

$$\widetilde{k} = \frac{\overline{\rho(u_i - \widetilde{u_i})(u_i - \widetilde{u_i})}}{2\overline{\rho}}$$

is the Favre averaged turbulent kinetic energy, and

$$\widetilde{\epsilon} = \frac{\overline{\rho\nu\left(\frac{\partial u_i}{\partial x_j} + \frac{\partial u_j}{\partial x_i}\right)\frac{\partial u_j}{\partial x_i}}}{\overline{\rho}}$$

is the Favre averaged dissipation rate of turbulent kinetic energy (Hinze, 1975). The Reynolds number based on the Taylor microscale is

$$\mathrm{Re}_\lambda = \frac{\sqrt{\frac{2}{3}\widetilde{k}}\lambda}{\widetilde{\nu}}.$$

This is shown as a function of x in Fig. 6 for several times: the initial condition is shown, as are those times for which visualizations were given in section 2.3.1 (7.5, 15 and 30 acoustic time units) along with the last time for which data is available at 90.0 acoustic time units.

The Taylor scale Reynolds number was initially around 60 in the cold fluid; however, the higher viscosity reduced this to only 20 in the flame. The effect of filtering the velocity fluctuations to zero at the outflow boundaries is apparent in that the Reynolds number drops dramatically to zero at the boundaries in the initial field. The diffusive nature of turbulence and the dilatation caused by heat release in the middle of the domain change this very quickly—by 7.5 time units; the Reynolds number at the boundaries rose to around 20. While a Taylor scale Reynolds number of 20 is very low, it can still be taken as an indication that there is turbulent motion present; this is roughly the Reynolds number of the turbulence in the reaction zone for all but the latest time shown.

The Kolmogorov length scale, which is

$$l_k = \left(\frac{\widetilde{\nu}^3}{\widetilde{\epsilon}}\right)^{1/4},$$

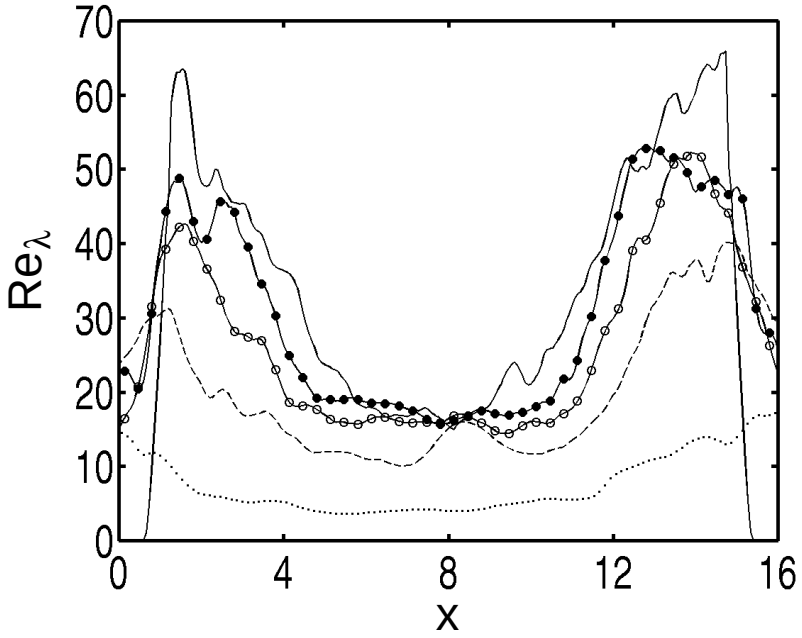

FIGURE 6. Favre averaged Taylor Reynolds number on planes of constant x through the mixing layer: —— $t = 0.0$; —●— $t = 7.5$; —○— $t = 15.0$; - - - - $t = 30.0$; ····· $t = 90.0$.

is shown in Fig. 7. This is initially almost constant in the domain except at the edges, where the dissipation is zero because the velocity fluctuations have been filtered out (this is why the Kolmogorov length shoots up to infinity at the edges). The Kolmogorov length in the middle of the domain, where the heat is released, rises with time much faster than it does at the edges of the domain. Initially the Kolmogorov length is somewhat smaller than the grid spacing (0.067) and this gets larger with time; this indicates that the turbulence was adequately resolved on the grid throughout the simulation.

The initial turbulent flow field did not exhibit any inertial range in its spectrum so it would be inappropriate to consider the integral length scale of the flow field. Instead, the dissipation length and time scales were examined. The dissipation length is

$$l_{\text{diss}} = \frac{u''^3}{\widetilde{\epsilon}}$$

and the dissipation time is

$$t_{\text{diss}} = \frac{l_{\text{diss}}}{u''},$$

where $u'' = \sqrt{\frac{2\widetilde{k}}{3}}$. These are shown in Fig. 8. The dissipation length is initially around $0.8L$ in the middle of the domain and just over $2.5L$ in the cold fluid near the edges; it is zero at the boundaries, but this is again due to the filtering of the fluctuations there. In time, the dissipation length appears to decay to around

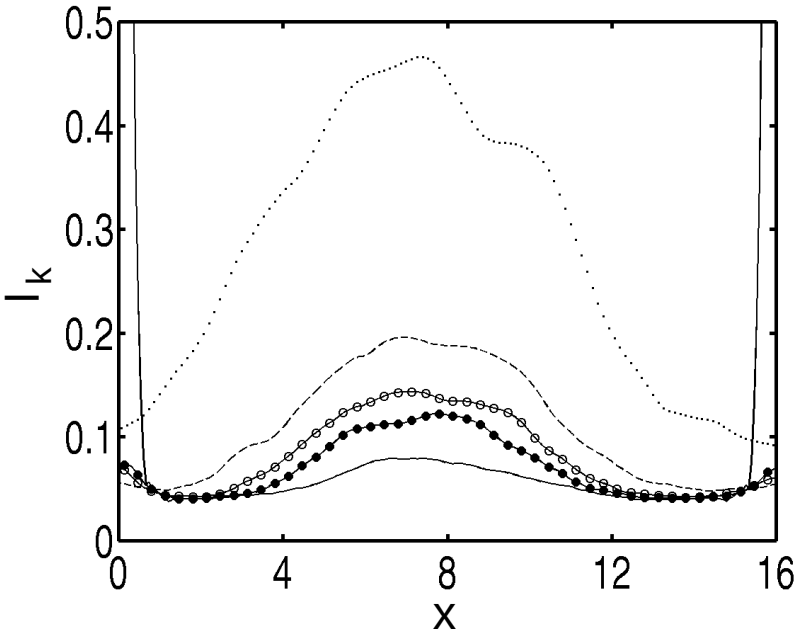

FIGURE 7. Favre averaged Kolmogorov length on planes of constant x through the mixing layer: —— $t = 0.0$; —●— $t = 7.5$; —○— $t = 15.0$; - - - - $t = 30.0$; ····· $t = 90.0$.

$0.7L$ throughout the domain. The dissipation time is initially very low—around 2 acoustic time units—in the middle of the domain, but exceeds 50 in the cold fluid. In time, the dissipation time increases to around 25 acoustic time units in the middle of the domain but remains around 45 at the edges. The dissipation length in the middle of the domain is initially about one order of magnitude larger than the Kolmogorov length. Only at 90 time units do these lengths become comparable. This is further evidence that the flow is turbulent albeit not very vigorous given the fairly long dissipation times.

The Favre averaged scalar dissipation is shown in Fig. 9a. Clearly, in the presence of turbulence the mean scalar dissipation is considerably larger in magnitude than the initial, laminar profile. The peak in scalar dissipation is at 7.5 time units and this decays slowly. Only when the turbulence has effectively decayed away, evidenced by the low Reynolds number, does the mean scalar dissipation return to near the initial laminar curve.

The Favre average of the temperature is shown in Fig. 9b. The peak mean temperature drops abruptly in the presence of turbulence; this is likely due more to the variance of mixture fraction that results from large scale mixing than to local changes in the flame. The peak mean temperature never approaches that of the initial curve although the increase in the area under the mean temperature curve with time indicates that the reactions are still clearly proceeding in earnest throughout the run.

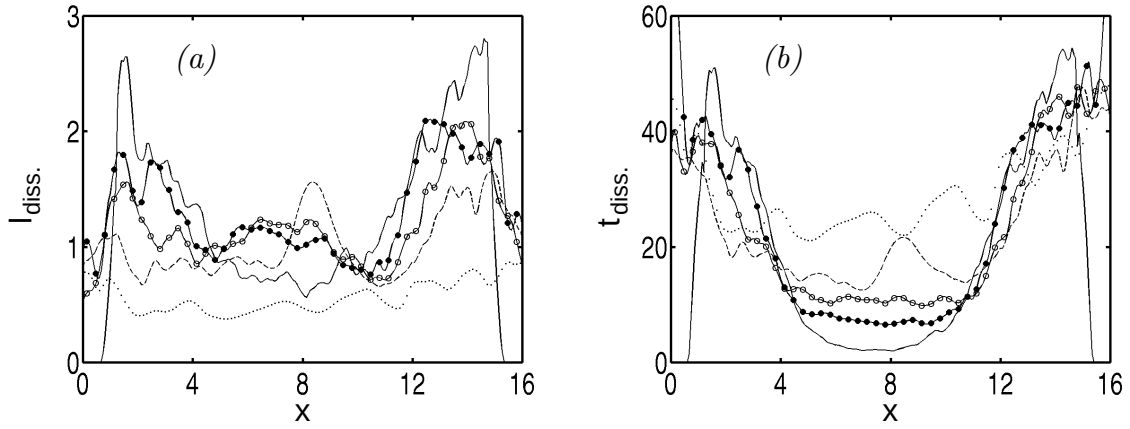

FIGURE 8. Favre averaged dissipation length (a) and time (b) on planes of constant x through the mixing layer: —— $t = 0.0$; —●— $t = 7.5$; —○— $t = 15.0$; - - - - $t = 30.0$; ····· $t = 90.0$.

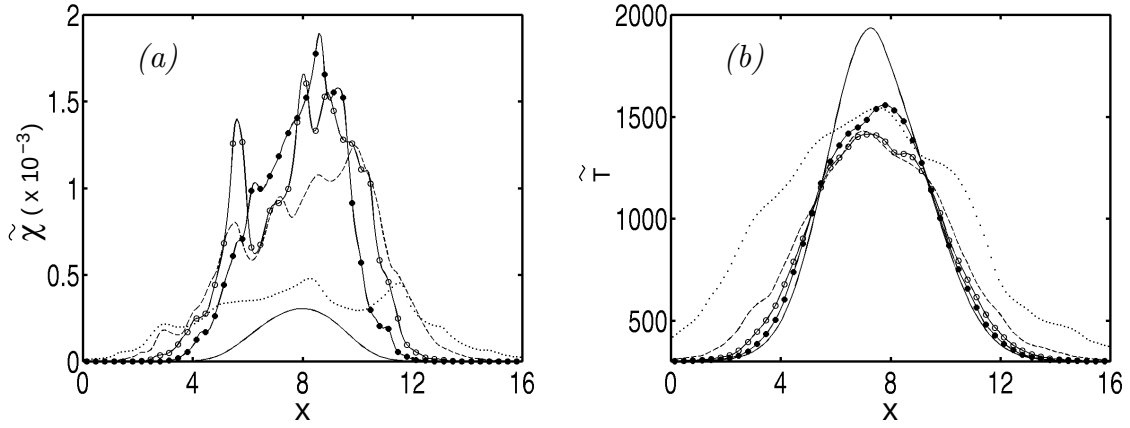

FIGURE 9. Favre averaged scalar dissipation rate (a) and temperature (b) on planes of constant x through the mixing layer: —— $t = 0.0$; —●— $t = 7.5$; —○— $t = 15.0$; - - - - $t = 30.0$; ····· $t = 90.0$.

2.3.4 Conditional reaction rates

In Fig. 10, the conditional averages of the reaction rates are compared to those predicted by evaluating the reaction rates with the conditionally averaged mass fractions, temperature, and density in the entire domain at 15 acoustic time units. This is a test of the validity of the first order CMC hypothesis, which is used to obtain closure for the chemical source terms in both the CMC and CSE approaches. The reaction rates for reactions I and II are predicted to within 5%. However, the under-prediction of reaction III is substantial—over 25%.

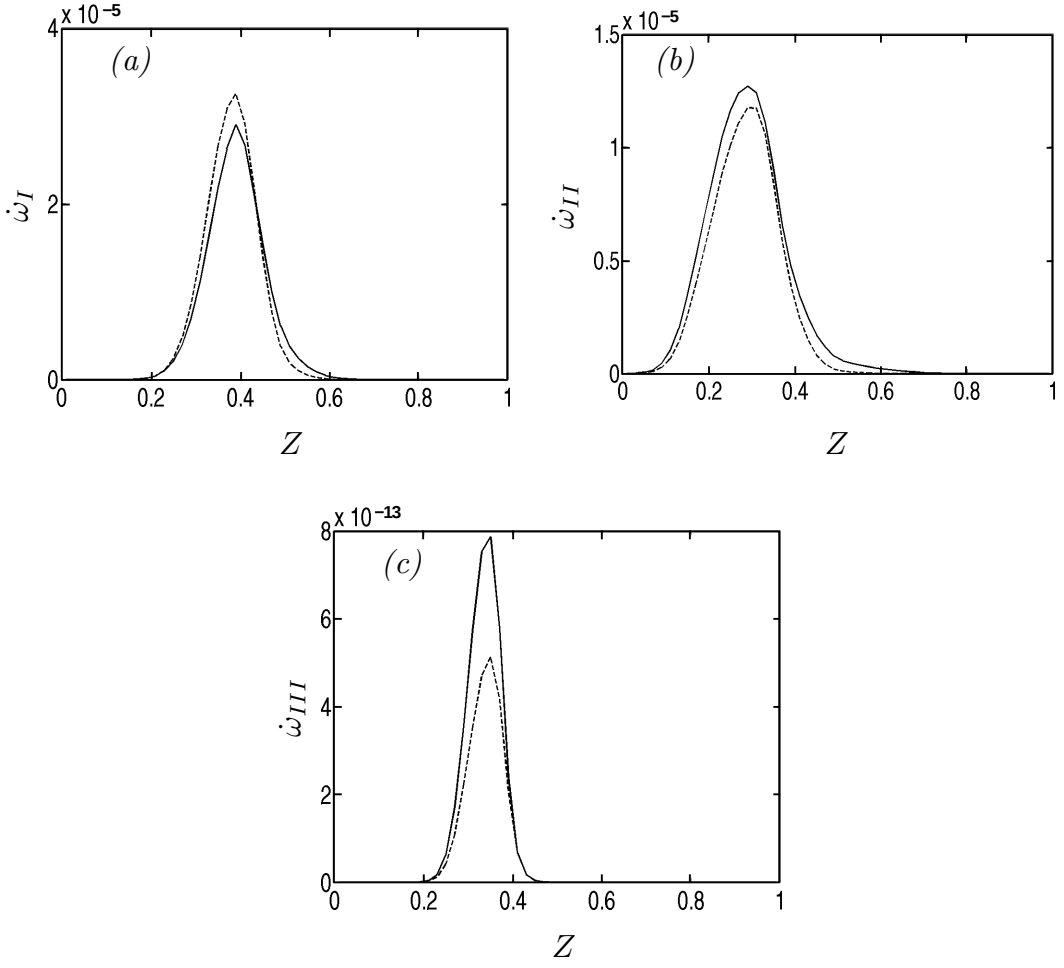

FIGURE 10. Comparison of conditionally averaged reaction rates to reaction rates predicted using the first order CMC approximation at 15 time units:
(a) ——— , $\langle\dot{\omega}_I(Y_J,T)|Z=\eta\rangle$; ····· , $\dot{\omega}_I(Q_J,\langle T|Z=\eta\rangle)$;
(b) ——— , $\langle\dot{\omega}_{II}(Y_J,T)|Z=\eta\rangle$; ····· , $\dot{\omega}_{II}(Q_J,\langle T|Z=\eta\rangle)$;
(c) ——— , $\langle\dot{\omega}_{III}(Y_J,T)|Z=\eta\rangle$; ····· , $\dot{\omega}_{III}(Q_J,\langle T|Z=\eta\rangle)$.

2.4 Discussion

Several interesting findings are seen in the previous section. These will now be discussed in greater detail.

2.4.1 Extinction effect

Non-premixed flames can be thought of as a competition between local chemical reaction and local mixing. At low values of local scalar dissipation (which is a direct measure for the rate of mixing), the reactions which consume fuel and oxidizer are limited by the mixing rate. As the local scalar dissipation increases, these chemical reaction rates will increase. When the local scalar dissipation rate becomes very large, the rate of diffusion of heat away from the reaction zone, the region of space in which chemical reaction is taking place, becomes large and can exceed the

rate at which chemical reaction replenishes that heat; the local temperature goes down. Since virtually all chemical reaction rates in flames are strongly temperature dependent, the reaction rates are slowed. If the high scalar dissipation persists for a sufficiently long time, these reactions can become quenched. Once this has occurred, even if the scalar dissipation subsides, the reaction rates will not recover, and re-ignition occurs either by a premixed front originating from non-extinguished gas adjacent to the region of local extinction or by auto-ignition.

This local extinction phenomenon is clearly evident in the sequence of Figs. 2-4. At 7.5 time units, the scalar dissipation peaks at a location where the temperature reaches a local saddle point, and yet reaction rates I and II are significant at the same location. It is only at 15.0 time units that these reaction rates appear to be quenched.

At this time, however, it is not yet clear whether the extinction events seen in the database are genuinely a result of low-temperature quenching of the reaction rates or an effect of the form of the steady-state expression for the Hydrogen radical. The form used contains an exponential term which is a surrogate for a sharp cut-off function of $Y_{\mathrm{Fu}}/Y_{\mathrm{Oxi}}$. It is conceivable that the extinction events were caused by depletion of the Hydrogen radical and that the low local temperatures are a consequence of extinction rather than the cause. This shall remain a question for future work.

2.4.2 Edge-flames

It is interesting to note that the flames at the edges of the extinction event seen in Figs. 3 and 4 do not exhibit triple flame structure. This was investigated carefully—where colormaps for the plots were manipulated so as to highlight even very low reaction rates—and found to be true for all of the times at which data was analyzed. It has not yet been possible to search through the fields at later times to establish if this is a persistent phenomenon. Furthermore, given the possibility that the extinction events may be caused by Hydrogen radical depletion rather than low-temperature quenching, it is possible that the lack of premixed branches is a consequence of the form of the reaction rates. In earlier simulations using different initial conditions (with the same chemical kinetic mechanism), premixed branches of triple flames were clearly evident; thus this seems an unlikely explanation. Alternatively, the lack of premixed branches on the edges of the reaction zones may be an indicator that the edge-flames are receding or that the local scalar dissipation is still so high that the premixed branches ordinarily associated with triple-flames have merged with the diffusion branch (Vervisch & Trouvé, 1998). This, too, will remain a question for future work.

2.4.3 NO production

It is also interesting to note the correlation between production of Nitric Oxide and peak temperature. Given the very large activation energy of this reaction, it would be expected that it would be sensitive to temperature. It also appears to be sensitive to the mass fraction of the Hydrogen radical.

2.4.4 Scatter plots

One important effect of the local extinction phenomenon is to cause considerable scatter in the scalar fields. This could pose considerable difficulty to moment closure methods such as CMC or CSE; conditional averages of most of the properties shown in Fig. 5 would fail to represent the wide scatter, and the mean reaction rates, which are highly sensitive non-linear functions of the scalar fields, would not be well represented by the first moment CMC closure hypothesis. Thus, local extinction phenomena, in particular their effect on scatter in the scalar fields, would likely necessitate either adding an additional conditioning variable to account for the physical process at the root of the scatter—such as the scalar dissipation—or the use of a second moment closure.

2.4.5 Favre averaged statistics

The Favre averages make clear the fact that the turbulent flow field is substantially influenced by the presence of the flame. This is true in the initial field as evidenced by the strong spatial dependence of the Taylor scale Reynolds number. It is also clear in the Kolmogorov length scale, which is almost constant across the layer in the initial field, but is almost five times greater in the middle of the layer, where the temperature peaks, than at the edges of the simulation after 90 time units. While the Kolmogorov length varies more across the layer as time progresses, the Reynolds number, dissipation length, and time all tend to become more evenly distributed.

The scalar dissipation and temperature plots (Figs. 9a and 9b) show how misleading mere Favre averages can be. In the scalar dissipation plot, the maximum mean scalar dissipation is almost one order of magnitude lower than the peak scalar dissipation seen in the visualizations (Figs. 2-4). If one were using a model that incorporated scalar dissipation into the prediction of reaction rates, such as CMC or laminar flamelets, one could conceivably under-predict the significance of extinction phenomena (which are clearly strongly dependent on scalar dissipation) by using only the mean scalar dissipation and neglecting fluctuations around that mean. The temperature plot shows an abrupt drop to around a 1500 K peak temperature, which is not evident in the visualizations. The drop in the Favre average of temperature appears to be primarily due to the out-of-plane folding across the layer. This highlights the difficulty in providing closure for the chemical source terms. One would grossly under-predict the reaction rates if one were to attempt to estimate these using the Favre averaged values directly.

2.4.6 Implications for modeling

The test of the validity of Conditional Moment Closure for the chemical source terms is encouraging. It would not be expected that single moment closure using only mixture fraction as a conditioning variable would give such agreement even in the presence of the extinction phenomena described above. Indeed, several modifications to the method have been proposed in order to improve closure for cases where extinction might occur. These include the addition of other conditioning variables (as in Bilger, 1991 and Bushe & Steiner, 1998) or the use of conditional

variances (as in Li & Bilger, 1993; Kronenburg *et al.*, 1998; Swaminathan & Bilger, 1998b).

While the closure appears to work well for two of the reactions, it appears to break down for the slower pollutant formation step. Since the activation energy of the Nitric Oxide formation reaction is very large, it is quite sensitive to variations in temperature. The considerable scatter in the temperature evident in Fig. 5b has a significant impact on this reaction. This indicates that a higher moment closure might be necessary although the potential to use scalar dissipation, with which variations in temperature appear to correlate strongly, as a second conditioning variable might improve closure as well.

3. Future work

Several issues remain to be addressed. A more detailed analysis of the affect of heat release on the flow field is needed so as to better describe the interaction of the flow with the chemical reactions. Further research into the edge flames present after extinction events will also be needed to attempt to establish the parameters which control whether or not triple flames form.

Ultimately, however, the purpose of the database was originally intended to be the validation of modeling, and it is this direction that attention will be focused in the near future. Already, the database has been used in *a priori* tests of models. Beyond the comparisons shown herewith, Cook and Bushe (1998) have used the database to test a new model for scalar dissipation for use in LES. The data is also being used to test the CSE approach in a RANS context. Model validation work is going to continue; in particular, *a priori* tests of the CSE approach for LES will be conducted and statistics relevant to second moment CMC closure will be extracted.

Acknowledgments

The authors wish to thank G. R. Ruetsch for providing the codes used in the development of this database. R. W. B. gratefully acknowledges the financial support of the Australian Research Council. The simulations were performed at the NAS facility of the NASA Ames Research Center.

REFERENCES

Bilger, R. W. 1980 Nonpremixed turbulent reacting flows. *Topics in Applied Physics.* **44,** Springer-Verlag, 65.

Bilger, R. W. 1991 Conditional moment methods for turbulent reacting flow using Crocco variable conditions. *Charles Kolling Laboratory Report,* Department of Mechanical Engineering, The University of Sydney, TN F-99

Bilger, R. W. 1993a Conditional moment closure for turbulent reacting flow. *Phys. Fluids A.* **5**(2)**,** 436.

Bilger, R. W. 1993b Conditional moment closure modeling and advanced laser measurements. In *Turbulence and Molecular Processes in Combustion,* T. Takeno (Ed), Elsevier, 267.

Bushe, W. K., Bilger, R. W. and Ruetsch, G. R. 1997 Incorporating realistic chemistry into direct numerical simulations of turbulent non-premixed combustion. *Annual Research Briefs,* Center for Turbulence Research, NASA Ames/Stanford Univ., 195.

Bushe, W. K. and Steiner, H. 1998 Conditional Moment Closure for Large Eddy Simulation of non-premixed turbulent reacting flows. *CTR Manuscript 170,* Center for Turbulence Research, NASA Ames/Stanford Univ.

Chen, J. H., Mahalingam, S., Puri, I. K. and Vervisch, L. 1992 Effect of finite-rate chemistry and unequal Schmidt numbers on turbulent non-premixed flames modeled with single-step chemistry. *Proceedings of the 1992 Summer Program,* Center for Turbulence Research, NASA Ames/Stanford University, 367.

Chen, J. H. and Echekki, T. 1996 Unsteady strain rate and curvature effects in turbulent premixed methane-air flames. *Combust. & Flame.* **106,** 184.

Cook, A. and Bushe, W. K. 1998 A subgrid-scale model for the scalar dissipation rate in nonpremixed combustion. *Proceedings of the 1998 Summer Program,* Center for Turbulence Research, NASA Ames/Stanford University*, to appear.*

Hinze, J. O. 1975 *Turbulence*, McGraw-Hill.

Klimenko, A. Y. 1990 Multicomponent diffusion of various admixtures in turbulent flow. *Fluid Dynamics.* **25,** 327.

Kronenburg, A., Bilger, R. W. and Kent, J. H. 1998 Second order Conditional Moment Closure for turbulent jet diffusion flames. *Twenty-seventh Symposium (International) on Combustion, The Combustion Institute, Pittsburgh, PA (to appear).*

Lele, S. 1992 Compact finite difference schemes with spectral-like resolution. *J. Comp. Phys.* **103,** 16.

Li, J. D. and Bilger, R. W. 1993 Measurement and prediction of the conditional variance in a turbulent reactive-scalar mixing layer. *Phys. Fluids A.* **5,** 12, 3255.

Peters, N. 1984 Laminar diffusion flamelet models. *Prog. Energy Combust. Sci.* **10,** 319.

Pitsch, H., and Peters, N. 1998 A Consistent Flamelet Formulation for Non-Premixed Combustion Considering Differential Diffusion Effects. *Combust. & Flame.* **114,** 26.

Poinsot, T., and Lele, S. 1992 Boundary conditions for direct simulations of compressible viscous flows. *J. Comp. Phys.* **101,** 104.

Ruetsch, G. R., and Maxey, M. R. 1991 Small-scale features of the vorticity and passive scalar fields in homogeneous isotropic turbulence. *Phys. Fluids.* **3,** 1587.

Ruetsch, G. R., Vervisch, L., and Liñán, A. 1995 Effects of heat release on triple flames. *Phys. Fluids.* **7,** 1447.

Smith, N. A. S. 1996 Conditional moment closure of mixing and reaction in turbulent nonpremixed combustion. *Annual Research Briefs,* Center for Turbulence Research, NASA Ames/Stanford Univ., 85.

Swaminathan, N. and Bilger, R. W. 1997 Direct numerical simulation of turbulent nonpremixed hydrocarbon reaction zones using a two-step reduced mechanism. *Comb. Sci. & Tech.* **127,** 167.

Swaminathan, N. and Bilger, R. W. 1998a Assessment of combustion submodels for turbulent nonpremixed hydrocarbon flames. *Combust. & Flame.* In press).

Swaminathan, N. and Bilger R. W. 1998b Conditional variance equation and its analysis. *Twenty-seventh Symposium (International) on Combustion, The Combustion Institute, Pittsburgh, PA (to appear).*

Tennekes, H. and Lumley, J. L. 1992 *A First Course in Turbulence*, MIT Press.

Vervisch, L. 1992 Study and modeling of finite rate chemistry effects in turbulent non-premixed flames. *Annual Research Briefs,* Center for Turbulence Research, NASA Ames/Stanford Univ., 411.

Vervisch, L. and Trouvé, A. 1998 LES modeling for lifted turbulent jet flames. *Proceedings of the 1998 Summer Program,* Center for Turbulence Research, NASA Ames/Stanford Univ., (to appear).

Williams, F. A. 1991 Overview of asymptotics for methane flames, in *Reduced Kinetic Mechanism and Asymptotic Approximations for Methane-Air Flames*, Springer-Verlag, New York, 68.